

# A $C^{18}O$ study of the origin of the power-law nature in the IMF

Norio Ikeda

Institute of Space and Astronautical Science/Japan Aerospace Exploration Agency, 3-1-1  
Yoshinodai, Sagamihara, Kanagawa 229-8510, Japan

`nikeda@isas.jaxa.jp`

and

Yoshimi Kitamura

Institute of Space and Astronautical Science/Japan Aerospace Exploration Agency, 3-1-1  
Yoshinodai, Sagamihara, Kanagawa 229-8510, Japan

Received \_\_\_\_\_; accepted \_\_\_\_\_

## ABSTRACT

We have performed  $C^{18}O$  ( $J=1-0$ ) mapping observations of a  $20' \times 20'$  area of the OMC-1 region in the Orion A cloud. We identified 65  $C^{18}O$  cores, which have mean radius, velocity width in FWHM, and LTE mass of  $0.18 \pm 0.03$  pc,  $0.40 \pm 0.15$  km s $^{-1}$ , and  $7.2 \pm 4.5 M_{\odot}$ , respectively. All the cores are most likely to be gravitationally bound by considering the uncertainty in the  $C^{18}O$  abundance. We derived a  $C^{18}O$  core mass function, which shows a power-law-like behavior above  $5 M_{\odot}$ . The best-fit power-law index of  $-2.3 \pm 0.3$  is consistent with those of the dense core mass functions and the stellar initial mass function (IMF) previously derived in the OMC-1 region. This agreement strongly suggests that the power-law form of the IMF has been already determined at the density of  $\sim 10^3$  cm $^{-3}$ , traced by the  $C^{18}O$  ( $J=1-0$ ) line. Consequently, we propose that the origin of the IMF should be searched in tenuous cloud structures with densities of less than  $10^3$  cm $^{-3}$ .

*Subject headings:* ISM: clouds — ISM: individual(Orion A) — stars: formation

## 1. Introduction

One of the most important observational features of the stellar initial mass function (IMF) is its power-law-like nature above  $1 M_{\odot}$ , as  $dN/dM \propto M^{-\gamma}$ . In the solar neighborhood, the power-law index  $\gamma$  seems to be greater than 2 (Salpeter 1955; Kroupa 2001), which characterizes the statistical properties of stars. In particular, both the total number and mass of stars are dominated by those of low-mass stars of  $\sim 1 M_{\odot}$ . It is natural to consider that the origin of the IMF shape is related to the mass distribution of its natal gas in molecular clouds. Many authors have investigated dense gas ( $10^{4-5} \text{ cm}^{-3}$ ) in molecular clouds by using (sub)millimeter dust continuum emission and/or molecular line emissions having high critical densities such as the  $\text{H}^{13}\text{CO}^+(J=1-0)$  and  $\text{N}_2\text{H}^+(J=1-0)$  lines (e.g., Motte et al. 1998; Reid & Wilson 2006; Nutter & Ward-Thompson 2007; Ikeda et al. 2007; Walsh et al. 2007; Enoch et al. 2008). They identified numerous cores that have typical sizes of  $0.05 - 0.1 \text{ pc}$  and masses of  $1 - 10 M_{\odot}$  in nearby ( $\leq 500 \text{ pc}$ ) star forming regions such as Orion, Ophiuchus, Perseus, and Serpens. The molecular line studies showed that the cores are gravitationally bound and are likely to produce stars. Moreover, they found that the core mass functions (CMFs) derived by using the dense gas tracers, referred to as DCMFs hereafter, seem to have power-law-like behaviors in high-mass parts, whose  $\gamma$  values are very similar to that of the IMF. One exception is that Kramer et al. (1998) found a significantly smaller  $\gamma$  value of 1.7 for the S140 and M17SW regions by using the  $\text{C}^{18}\text{O}(J=2-1)$  line with a high critical density comparable to that of  $\text{H}^{13}\text{CO}^+(1-0)$ . Considering that the power-law form of the IMF has been already determined at the formation stage of the cores with the densities of  $10^{4-5} \text{ cm}^{-3}$ , it is likely that more tenuous structures of molecular clouds have a key to understanding the origin of the power-law nature of the IMF.

It has been suggested that the mass functions in the tenuous gas structures are different

from the DCMFs. Kramer et al. (1998) carried out a systematic study of the mass functions in the tenuous gas structures of  $10^3 \text{ cm}^{-3}$  or less by using the  $^{12}\text{CO}(2-1)$ ,  $^{13}\text{CO}(1-0; 2-1)$ , and  $\text{C}^{18}\text{O}(1-0)$  lines in various molecular clouds. They showed that their mass functions seem to have a common power-law form, and the  $\gamma$  value of  $1.7 \pm 0.1$  is significantly smaller than those of the DCMFs and the IMF. Heithausen et al. (1998) derived  $^{12}\text{CO}(J=1-0, 2-1)$  mass functions in the MCLD 123.5+24.9 and Polaris Flare regions and found that  $\gamma = 1.8 \pm 0.1$ . Wong et al. (2008) found  $\gamma = 1.7$  in the  $\text{C}^{18}\text{O}(J=1-0)$  mass function of RCW 106. These facts mean that the power-law index of the IMF may be originated in the formation process of the dense gas of  $10^{4-5} \text{ cm}^{-3}$  from the tenuous gas of  $10^{2-3} \text{ cm}^{-3}$ . However, one should be careful in comparing the  $\gamma$  value of the tenuous gas mass function to those of the DCMFs and the IMF. This is because the tenuous gas mass functions described above were derived by the spatial resolutions larger than 0.1 pc, which cannot resolve star-forming cores, and/or by using optically-thick tracers such as  $^{12}\text{CO}$  and  $^{13}\text{CO}$ . To fairly compare the tenuous gas mass function with the DCMFs and the IMFs, one should achieve higher spatial resolutions than 0.1 pc and use optically-thin tracers.

In this paper, we present a CMF derived by  $\text{C}^{18}\text{O}(J=1-0)$  mapping observations of the OMC-1 region, which is located at the center of the Orion A Giant Molecular Cloud. The aim of this study is to examine whether or not the common power-law form between the DCMFs and the IMF has been already determined in the tenuous gas of  $\leq 10^3 \text{ cm}^{-3}$  by focusing on the power-law index  $\gamma$  in the high-mass part of the CMF. The  $\text{C}^{18}\text{O}(J=1-0)$  molecular line emission is suitable for deriving the CMF (e.g., Tachihara et al. 2002) because the line has a relatively small critical density of  $\sim 10^3 \text{ cm}^{-3}$  (Ungerechts et al. 1997) and is typically optically thin (see §3.2). The OMC-1 region is one of the best regions to investigate the CMF, because the IMF of the associated Orion Nebula Cluster (ONC) has been derived (Hillenbrand 1997; Muench et al. 2002), and because the power-law form of the  $\text{H}^{13}\text{CO}^+$  DCMF is shown to be quite similar to that of the ONC IMF by Ikeda et al.

(2007). Furthermore, at the distance to the Orion A cloud of 480 pc (Genzel et al. 1981) we can easily resolve the cores with radii of  $\sim 0.1$  pc. As described in §2, the mapping observations have been done with the effective spatial resolution of  $26''.4$  ( $= 0.06$  pc), which is high enough to resolve the dense cores in the OMC-1 region (Ikeda et al. 2007).

## 2. Observations

The mapping observations were carried out in the period from January to February 2008 by using the Nobeyama 45 m radio telescope. The mapping covered a central  $20' \times 20'$  area of the OMC-1 region. The position of the Orion-KL object ( $5^{\text{h}}35^{\text{m}}14^{\text{s}}.2$ ,  $-5^{\circ}22'22''$ ; J2000) was taken to be the center of the mapping region. Note that the region was selected to be the same as that in the  $\text{H}^{13}\text{CO}^+$  DCMF study by Ikeda et al. (2007). Using the On-The-Fly method (Sawada et al. 2008), we swept the mapping region by raster scan with a scan speed of the telescope of  $52$  arcsec  $\text{s}^{-1}$ . To reduce scanning effects, we scanned in both the RA and Dec directions. At the frequency of the  $\text{C}^{18}\text{O}(J=1-0)$  emission ( $109.782182$  GHz; Ungerechts et al. 1997), the half power beam width,  $\Delta\theta_{\text{HPBW}}$ , and main beam efficiency,  $\eta$ , of the telescope were  $14''$  and  $0.4$ , respectively. At the front end, we used the 25-BEam Array Receiver System (BEARS) in double-sideband mode, which has  $5 \times 5$  beams separated by  $41''.1$  in the plane of the sky (Sunada et al. 2000; Yamaguchi et al. 2000). The 25 beams have beam-to-beam variations of about 10% in both beam efficiency and sideband ratio. To correct for the beam-to-beam gain variations, we calibrated the intensity scale of each beam using a 100 GHz SIS receiver (S100) with a single-sideband filter. At the back end, we used 25 sets of 1024 channel autocorrelators (ACs), which have a velocity resolution of  $0.104$  km  $\text{s}^{-1}$  at 110 GHz (Sorai et al. 2000). Since the data dumping time of the ACs was 0.1 s, the spatial data sampling interval on the sky plane was  $5.2''$ . The interval corresponds to  $0.35\Delta\theta_{\text{HPBW}}$ , and satisfies the Nyquist theorem. The

telescope pointing was checked every 1.5 hours by observing the SiO ( $v=1, J=1-0$ ; 43.122 GHz) maser source Orion KL. The pointing accuracy was better than  $3''$ . To construct an  $\alpha\text{-}\delta\text{-}v_{\text{LSR}}$  data cube, we used a Gaussian function as a gridding convolution function (GCF) to integrate the spectra which were taken with a very high spatial sampling rate of  $5.2''$ . We adopted  $22''.5$  as the size of the GCF in full width at half maximum. The resultant effective spatial resolution of the cube,  $\Delta\theta_{\text{eff}}$ , becomes  $26''.4$ . During the observations, the system noise temperature ranged from 295 to 429 K with a mean value of 351 K. Therefore, we have an RMS noise level of the data cube of 0.18 K in  $T_{\text{A}}^*$ .

### 3. Results

#### 3.1. $\text{C}^{18}\text{O}(J=1-0)$ Total Map

Figure 1 shows the total integrated intensity map of the  $\text{C}^{18}\text{O}(J=1-0)$  emission. The map shows that the OMC-1 region is elongated along the north-south direction. This elongated structure is a part of the Integral Shaped Filament (ISF; Bally et al. 1987), which is a global structure of the northern part of the Orion A cloud. Previously, Dutrey et al. (1991) obtained the  $\text{C}^{18}\text{O}(J=1-0)$  map of the ISF with a spatial resolution 6 times coarser than ours. Although the overall feature of our map is consistent with theirs, our map reveals a number of 0.1 pc-scale sub-structures owing to our higher spatial resolution. Such a clumpy structure is also seen in the  $\text{H}^{13}\text{CO}^+$  map of the OMC-1 region (Ikeda et al. 2007), which traces the dense gas of  $\sim 10^4 \text{ cm}^{-3}$ , one order of magnitude higher than  $\sim 10^3 \text{ cm}^{-3}$  traced by the  $\text{C}^{18}\text{O}$  line.

One distinct difference between the  $\text{C}^{18}\text{O}$  and  $\text{H}^{13}\text{CO}^+$  maps is that the  $\text{C}^{18}\text{O}$  map seems less clumpy than the  $\text{H}^{13}\text{CO}^+$  one, though the overall features of the two maps are similar to each other. In the  $\text{H}^{13}\text{CO}^+$  map, the ISF seems to mainly consist of the 0.1

pc-scale cores and the large-scale diffuse component seems minor. On the contrary, the diffuse component dominates the C<sup>18</sup>O map, and the clumpy structure seems less distinct than that in the H<sup>13</sup>CO<sup>+</sup> map. In addition, the diffuse component of the C<sup>18</sup>O map appears to be more extended than that of the H<sup>13</sup>CO<sup>+</sup> one. Actually, the total mass of the C<sup>18</sup>O emission above the 2  $\sigma$  level is estimated to be 1500  $M_{\odot}$  (see §3.2 for the mass estimate) and is 1.5 times larger than that of the H<sup>13</sup>CO<sup>+</sup> emission in the same region ( $\sim 1000 M_{\odot}$ ; Ikeda et al. 2007). These facts support that the C<sup>18</sup>O emission traces more tenuous gas of the cloud than the H<sup>13</sup>CO<sup>+</sup> emission.

### 3.2. Identification of C<sup>18</sup>O Cores and Estimation of the Core Properties

Following the H<sup>13</sup>CO<sup>+</sup> DCMF study in the OMC-1 region (Ikeda et al. 2007), we applied the `clumpfind` algorithm (Williams et al. 1994) to the C<sup>18</sup>O three-dimensional ( $\alpha$ - $\delta$ - $v_{\text{LSR}}$ ) data. For the input parameter for the algorithm,  $\Delta T$  in Williams et al. (1994), we adopted 0.36 K, i.e., the 2  $\sigma$  noise level of the cube data. Since the algorithm treats the contour levels of  $n\Delta T$  with  $n = 1, 2, 3, \dots$ , the threshold level is equal to the lowest contour level of  $\Delta T$ . Williams et al. (1994) showed that the 2  $\sigma$  noise level is optimal for  $\Delta T$  to extract clump and/or core structures from the cube data and to recover the physical properties of them, including the CMF. Recently, Pineda et al. (2009) examined more wider ranges of  $\Delta T$  (from 3 to 20  $\sigma$ ) than Williams et al. (1994) did and found that the mass functions of cloud sub structures specific to the adopted  $\Delta T$  have power-law indices depending on  $\Delta T$ , especially for higher  $\Delta T$  ( $> 5 \sigma$ ), suggesting the hierarchical nature of a molecular cloud. In this study, however, we focus our attention on the cores, corresponding to the 0.1 pc-scale hierarchical level directly related to star formation. Therefore, we prefer to use the `clumpfind` algorithm with the optimal  $\Delta T$  of the 2  $\sigma$  noise level confirmed by Williams et al. (1994) (see also §4). Note that we adopted the grid spacing of the cube

data of  $26''.4$ , equal to  $\Delta\theta_{\text{eff}}$ , i.e., full-beam sampling. This is because Williams et al. (1994) determined the optimal  $\Delta T$  of the  $2\sigma$  level for the full-beam sampling case. We also followed the additional criteria introduced in Ikeda et al. (2007) to reject ambiguous or fake core candidates whose size and velocity width are smaller than the spatial and velocity resolutions, respectively. As a result, we identified 65 cores. The total number of the  $\text{C}^{18}\text{O}$  cores is comparable to that of the  $\text{H}^{13}\text{CO}^+$  cores of 57 in the same region.

We estimated the radius  $R_{\text{core}}$ , velocity width in FWHM  $dv_{\text{core}}$ , LTE mass  $M_{\text{LTE}}$ , virial mass  $M_{\text{vir}}$ , and mean density  $\bar{n}$  of the  $\text{C}^{18}\text{O}$  cores. The definitions of these parameters are the same as those in Ikeda et al. (2007). In this study,  $\Delta\theta_{\text{eff}} = 26''.4$  and  $dv_{\text{spec}} = 0.104 \text{ km s}^{-1}$ . In the mass estimate, we adopted  $\eta = 0.4$  and  $T_{\text{ex}} = 20\text{K}$  (Cesaroni & Wilson 1994). For the fractional abundance of  $\text{C}^{18}\text{O}$  relative to  $\text{H}_2$ ,  $X_{\text{C}^{18}\text{O}}$ , we adopted  $1.7 \times 10^{-7}$  (Frerking et al. 1982). In addition, we confirmed that the  $\text{C}^{18}\text{O}(J=1-0)$  emission is optically thin. We observed the  $^{13}\text{CO}(J=1-0)$  emission (110.201 GHz) toward 25 positions in the OMC-1 region including the most intense  $\text{C}^{18}\text{O}$  peak at the Orion-S object ( $\alpha = 5^{\text{h}}35^{\text{m}}13^{\text{s}}$ ,  $\delta = -5^{\circ}24'30''$ ). We derived the optical depth of the  $\text{C}^{18}\text{O}$  emission  $\tau_{\text{C}^{18}\text{O}}$  by considering the terrestrial abundance ratio of  $[^{13}\text{C}^{16}\text{O}]/[^{12}\text{C}^{18}\text{O}]$  of 5.5, and found that  $\tau_{\text{C}^{18}\text{O}} \ll 1$  at all the 25 positions. Therefore, assuming the  $\text{C}^{18}\text{O}$  emission is optically-thin all over the observed area, we have

$$M_{\text{LTE}} = 5.0 \times 10^{-2} \left( \frac{X_{\text{C}^{18}\text{O}}}{1.7 \times 10^{-7}} \right)^{-1} T_{\text{ex}} e^{5.27/T_{\text{ex}}} \left( \frac{D}{480\text{pc}} \right)^2 \left( \frac{\Delta\theta_{\text{eff}}}{26''.4} \right)^2 \left( \frac{\eta}{0.4} \right)^{-1} \left( \frac{\sum_i T_{\text{A},i}^* \Delta v_i}{\text{K km s}^{-1}} \right) M_{\odot}, \quad (1)$$

where  $\sum_i T_{\text{A},i}^* \Delta v_i$  is the total integrated intensity of the core.

The mean values with standard deviation of  $R_{\text{core}}$ ,  $dv_{\text{core}}$ , and  $M_{\text{LTE}}$  are  $0.18 \pm 0.03 \text{ pc}$ ,  $0.40 \pm 0.15 \text{ km s}^{-1}$ , and  $7.2 \pm 4.5 M_{\odot}$ , respectively. These are consistent with those of the  $\text{H}^{13}\text{CO}^+$  cores of  $0.15 \pm 0.04 \text{ pc}$ ,  $0.58 \pm 0.23 \text{ km s}^{-1}$ , and  $15 \pm 16 M_{\odot}$ . The mean value of  $\bar{n}$  of  $(4.8 \pm 1.6) \times 10^3 \text{ cm}^{-3}$  is comparable to the critical density of the  $\text{C}^{18}\text{O}(J=1-0)$  line and is

one order of magnitude smaller than that of the  $\text{H}^{13}\text{CO}^+$  cores of  $(3.3\pm 1.8)\times 10^4 \text{ cm}^{-3}$ . The total mass of the  $\text{C}^{18}\text{O}$  cores is  $468 M_{\odot}$ , 30% of the total mass traced by the  $\text{C}^{18}\text{O}$  emission (see §3.1). This fraction is a half of that for the  $\text{H}^{13}\text{CO}^+$  case of 60 % (Ikeda et al. 2007, 2009), supporting that the  $\text{C}^{18}\text{O}$  emission is dominated by the diffuse component, compared with the  $\text{H}^{13}\text{CO}^+$  emission.

All the  $\text{C}^{18}\text{O}$  cores are likely to be gravitationally bound and have the potential for forming stars as well as the  $\text{H}^{13}\text{CO}^+$  cores. Figure 2 shows that the  $\text{C}^{18}\text{O}$  cores, except for one core with the smallest mass of  $1.3 M_{\odot}$ , are distributed around the line of  $M_{\text{vir}}/M_{\text{LTE}} = 1$  as well as the  $\text{H}^{13}\text{CO}^+$  cores. The virial ratio,  $M_{\text{vir}}/M_{\text{LTE}}$ , has a mean value of  $1.1\pm 0.8$  and the maximum value of 2.6. Even if we take the maximum value, the  $\text{C}^{18}\text{O}$  cores can be under virial equilibrium by considering the uncertainty in  $X_{\text{C}^{18}\text{O}}$  of a factor 3. On the other hand, the minimum-mass core has the smallest virial ratio of 0.03, indicating certainly self-gravitating. Although the core is located around the map center of  $\alpha = 5^{\text{h}}35^{\text{m}}13^{\text{s}}$ ,  $\delta = -5^{\circ}23'19''$ , the core is just on the border of the core identification (see §3.2 and Ikeda et al. 2007) and might have large uncertainties in its physical parameters. Even if the core would be an unresolved one, it never affects our discussion on the power-law nature in the high-mass part of the CMF, as in §4.

#### 4. $\text{C}^{18}\text{O}$ CMF and Comparison with the DCMFs and the IMF

Figure 3 shows the  $\text{C}^{18}\text{O}$  CMF. The CMF has a turnover at around  $5 M_{\odot}$ , and a power-law like shape in the high-mass part above the turnover. Above  $5 M_{\odot}$ , we applied a single power-law function by considering the statistical uncertainties and found that the best-fit power-law index  $\gamma$  is  $2.3\pm 0.3$ . Furthermore, we confirmed that the  $\gamma$  value is insensitive to the input parameter of the `clumpfind`,  $\Delta T$ . We checked the algorithm by changing the step size (i.e., the contour interval) and the threshold level (i.e., the lowest

contour level) independently, as shown in Figure 4. Note that the parameter ranges were limited so that the number of the identified cores could be large enough to construct the CMF. Figure 4 clearly shows that all the  $\gamma$  values are consistent with the best-fit value of 2.3 within the uncertainties.

Before the comparison with the DCMFs and the IMF, we correct the C<sup>18</sup>O CMF for the confusion effect using the model by Ikeda et al. (2009). The mass density of the low-mass cores of  $< 5M_{\odot}$ ,  $\rho_{\text{cube}}$ , in the C<sup>18</sup>O cube data is a key parameter in the confusion model and is estimated to be  $40.0 M_{\odot} \text{ pc}^{-2} \text{ km}^{-1} \text{ s}$ . The  $\rho_{\text{cube}}$  value is considerably smaller than that for the H<sup>13</sup>CO<sup>+</sup> cores in the OMC-1 region of  $99.0 M_{\odot} \text{ pc}^{-2} \text{ km}^{-1} \text{ s}$  (Ikeda et al. 2009). This difference probably corresponds to the fact that the C<sup>18</sup>O map is less clumpy than the H<sup>13</sup>CO<sup>+</sup> one, as stated in §3.1. The total mass misidentified by the confusion effect is estimated to be  $123 M_{\odot}$ , and the confusion-corrected CMF is reconstructed by adding 45 misidentified cores to the low-mass part below  $5 M_{\odot}$ . Here we exclude the minimum-mass bin of  $2 M_{\odot}$  only for the minimum-mass core, because the detection of the minimum-mass core could be marginal as stated in §3.2 and because the statistical uncertainty of the mass bin is large compared to the other bins below the turnover. Note that the confusion effect does not considerably affect the shape of the high-mass part of the CMF, even if we include the minimum-mass bin in the correction. In other words, our discussion about the power-law index  $\gamma$  in the high-mass part of the CMF is not considerably changed by the confusion effect.

In Figure 3 we also show the confusion-corrected C<sup>18</sup>O CMF. Although the shape in the low-mass part of the corrected CMF is considerably changed, the  $\gamma$  value in the high-mass part is consistent with that in the observed CMF within the uncertainties; we applied a single power-law function to the corrected CMF and obtained the best-fit  $\gamma$  value of  $2.4 \pm 0.2$ .

We have the  $\gamma$  value of the corrected  $\text{C}^{18}\text{O}$  CMF of  $2.4 \pm 0.2$ , which is quite consistent with those of the DCMFs. The  $\gamma$  value of the  $\text{H}^{13}\text{CO}^+$  DCMF corrected for the confusion effect was measured to be  $2.2 \pm 0.1$  (Ikeda et al. 2007). Nutter & Ward-Thompson (2007) derived the  $850 \mu\text{m}$  dust continuum DCMF in Orion and found that the best-fit  $\gamma$  is  $2.2 \pm 0.2$ . Furthermore, our  $\gamma$  value agrees well with that of the IMF within the uncertainties. Muench et al. (2002) derived the IMF of the Trapezium cluster, which is the center portion of the ONC, from the  $K$ -band luminosity function and found that  $\gamma = 2.2$ , as shown in Figure 3. The agreement between the  $\text{C}^{18}\text{O}$  CMF and the IMF suggests that, at least in the OMC-1 region in the Orion A cloud, the power-law form of the IMF with  $\gamma \geq 2$  has been already determined at the formation time of the tenuous structure with density of  $\sim 10^3 \text{ cm}^{-3}$ .

In future works, we propose observations using molecular lines having lower critical densities, such as  $^{12}\text{CO}(J=1-0)$  and  $^{13}\text{CO}(J=1-0)$ , or thermal dust continuum emission. Telescopes in orbit with spatial resolution of  $< 1'$  such as the Akari (Murakami et al. 2007) and Herschel satellites would be preferable to seek the origin of the IMF in the tenuous structures of molecular/atomic interstellar clouds (e.g., Toth et al. 2000).

For helping us in our observations and data reduction, we thank the staff of the Nobeyama Radio Observatory, that is a branch of the National Astronomical Observatory of Japan, National Institute of Natural Sciences. We also acknowledge an anonymous referee for valuable comments that improved the paper. This work is supported by a Grant-in-Aid for Scientific Research (A) from the Ministry of Education, Culture, Sports, Science and Technology of Japan (No. 19204020).

## REFERENCES

- Bally, J., Langer, W. D., Stark, A. A. & Wilson, R. W. 1987, *ApJ*, 312, L45
- Cesaroni, R. & Wilson, T. L. 1994, *A&A*, 281, 209
- Dutrey, A., Langer, W. D., Bally, J., Duvert, G., Castets, A. & Wilson, R. W. 1991, *A&A*, 247, 9
- Enoch, M. L., Evans, N. J. II, Sargent, A. I., Glenn, J., Rosolowsky, E. & Myers, P. 2008, *ApJ*, 684, 1240
- Frerking, M. A., Langer, W. D. & Wilson, R. W. 1982, *ApJ*, 262, 590
- Genzel, R., Reid, M. J., Moran, M. J. & Downes, D. 1981, *ApJ*, 244, 884
- Heithausen, A., Bensch, F., Stutzki, J., Falgarone, E. & Panis, J. F. 1998, *A&A*, 331, 65
- Hillenbrand, L. A. 1997, *AJ*, 113, 173
- Ikeda, N., Sunada, K. & Kitamura, Y. 2007, *ApJ*, 665, 1194
- Ikeda, N., Kitamura, Y. & Sunada, K. 2009, *ApJ*, 691, 1560
- Kramer, C., Stutzki, J., Röhrig, R. & Corneliussen, U. 1998, *A&A*, 329, 249
- Kroupa, P. 2001, *MNRAS*, 322, 231
- Motte, F., André, P. & Neri, R. 1998, *A&A*, 336, 150
- Muench, A. A., Lada, E. A. & Lada, C. J. 2002, *ApJ*, 573, 366
- Murakami, H. et al. 2007, *PASJ*, 59, 369
- Nutter, D. & Ward-Thompson, D. 2007, *MNRAS*, 374, 1413

- Pineda, J. E., Rosolowsky, E. W. & Goodman, A. A. 2009, *ApJ*, 699, L134
- Reid, M. A. & Wilson, C. D. 2006, *ApJ*, 650, 970
- Salpeter, E. E. 1955, *ApJ*, 121, 161
- Sawada, T., Ikeda, N., Sunada, K., Kuno, N., Kamazaki, T., Morita, K-I, Kurono, Y., et al. 2008, *PASJ*, 60, 445
- Sorai, K., Sunada, K., Iwasa, T., Tanaka, T., Natori, K. & Onuki, H. 2000, *Proc. SPIE*, 4015, 86
- Sunada, K., Yamaguchi, C., Nakai, N., Sorai, K., Okumura, S. & Ukita, N. 2000, *Proc. SPIE*, 4015, 237
- Tachihara, K., Onishi, T., Mizuno, A. & Fukui, Y. 2002, *A&A*, 385, 909
- Toth, L. V. et al. 2000, *A&A*, 364, 769
- Ungerechts, H., Bergin, E. A., Goldsmith, P. F., Irvine, W. M., Schloerb, F. P. & Snell, R. L. 1997, *ApJ*, 482, 245
- Walsh, A. J., Myers, P. C., Di Francesco, J., Mohanty, S., Bourke, T. L., Gutermuth, R. & Wilner, D. 2007, *ApJ*, 655, 958
- Williams, J. P., de Geus, E. J. & Blitz, L. 1994, *ApJ*, 428, 693
- Wiseman, J. J. & Ho, P. T. P. 1998, *ApJ*, 502, 676
- Wong, T. et al. 2008, *MNRAS*, 386, 1069
- Yamaguchi, C., Sunada, K., Iizuka, Y., Iwashita, H. & Noguchi, T. 2000, *Proc. SPIE*, 4015, 614

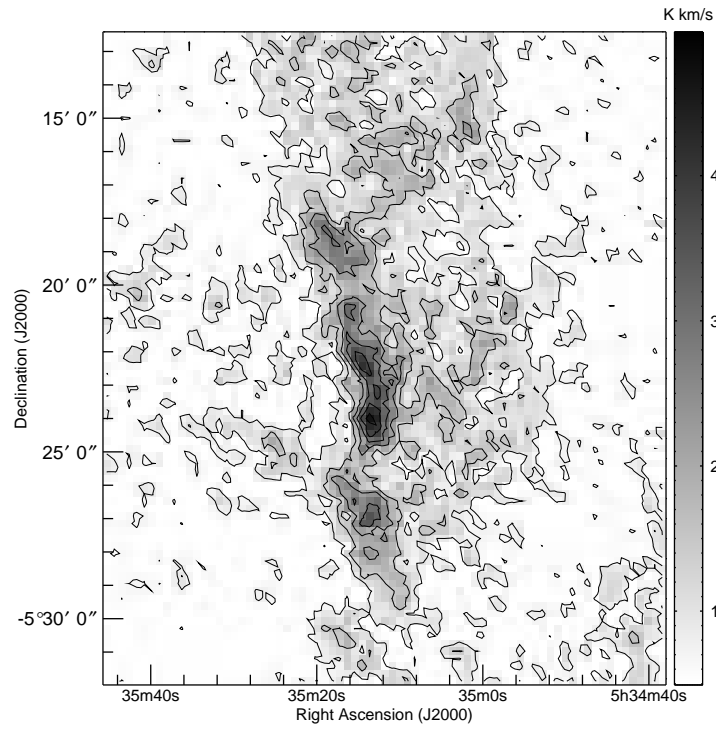


Fig. 1.— Total integrated intensity map of the  $C^{18}O(J = 1 - 0)$  emission ( $v_{\text{LSR}} = 0.2 - 15.0$  km s<sup>-1</sup>) in the OMC-1 region. The contour intervals are 0.74 K km s<sup>-1</sup> (corresponding to  $2\sigma$ ) starting at 0.74 K km s<sup>-1</sup>. The gray scale bar is shown at the right-hand side of the panel.

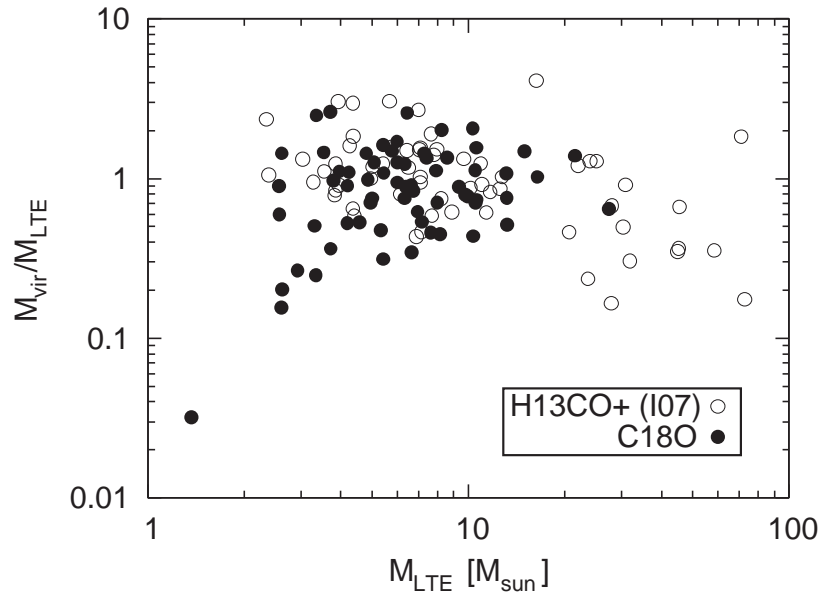


Fig. 2.— Virial ratio ( $M_{\text{vir}}/M_{\text{LTE}}$ )-mass relation of the  $\text{C}^{18}\text{O}$  cores (filled circles). The open circles show the same relation of the  $\text{H}^{13}\text{CO}^+$  cores in the OMC-1 region (Ikeda et al. 2007).

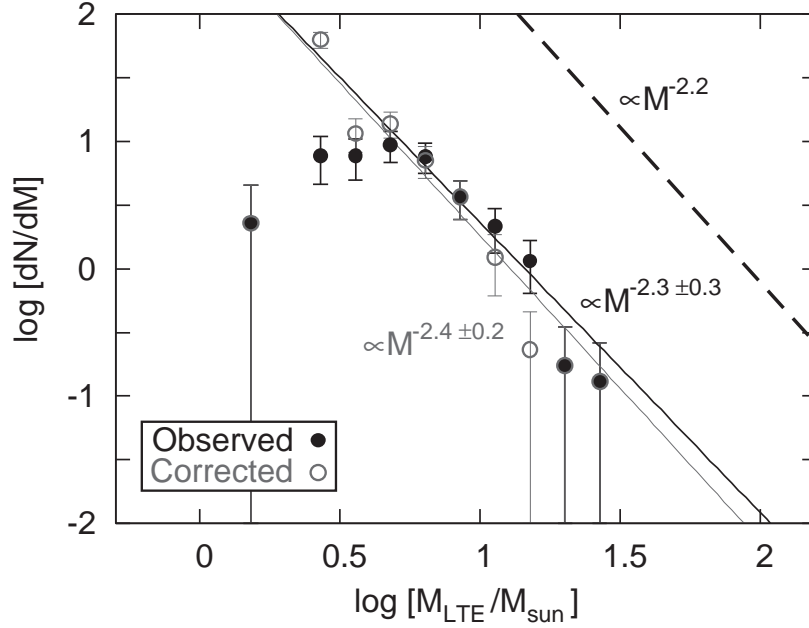


Fig. 3.— Observed and confusion-corrected  $\text{C}^{18}\text{O}$  CMFs are shown by the thick-color filled and thin-color open circles, respectively. The error bars indicate the statistical uncertainty of  $\sqrt{N}$ , where  $N$  is the core number in each bin. The thick- and thin-color solid lines shows the best-fit power-law functions in the high-mass part above  $5 M_{\odot}$  for the observed and corrected CMFs, respectively (see §4). The slope in the high-mass part of the IMF of the Trapezium cluster (Muench et al. 2002) is also shown by the dashed line. Note that the  $dN/dM$  value of the IMF is arbitrary scaled.

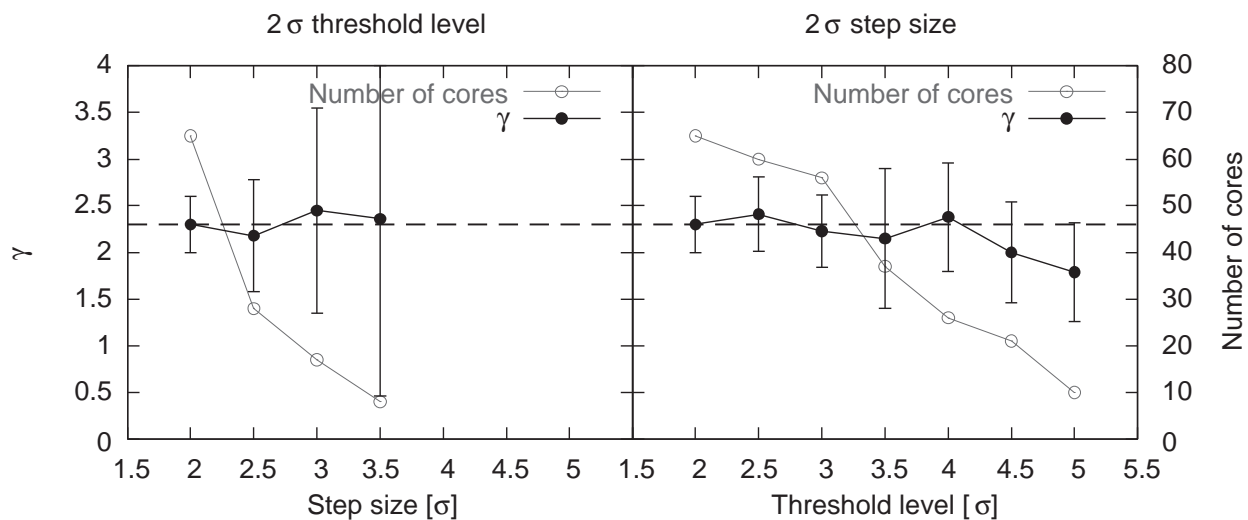


Fig. 4.— Number of the identified  $C^{18}O$  cores (thin-color symbols) and power-law index  $\gamma$  of the resultant CMF (thick-color symbols) are shown as a function of the step size and the threshold level in the left and right panels, respectively. The y-axis on the left- and right-hand sides of each panel indicate the  $\gamma$  values and the core numbers, respectively. The vertical error bars with the  $\gamma$  symbols correspond to the uncertainties in power-law fitting. The horizontal dashed line shows the  $\gamma$  value obtained by the optimal parameters of the  $2\sigma$  step size and the  $2\sigma$  threshold level (see Figure 3).